Journal of Asian Concrete Federation
Vol. 8, No. 1, pp. 1-15, June. 2022
ISSN 2465-7964 / eISSN 2465-7972
DOI http://dx.doi.org/10.18702/acf.2022.6.8.1.1

Technical Paper

Finite element analysis of steel-concrete composite connection with prefabricated permanent steel form

Hyunjin Ju, Deuckhang Lee*, Dong-Uk Choi

(Received: November 11, 2021; Accepted: March 18, 2022; Published online: June 30, 2022)

Abstract: Composite structural members are widely used due to superior performance to traditional structural members consisting of either concrete or steel material. This study proposes steel-concrete composite beam-column connections utilizing prefabricated permanent steel form and presents a finite element analysis to verify the structural performance of the system, which is based on the experimental data conducted under cyclic loading protocol simulating seismic action. Five different design specimens are covered where the key variables include the asymmetric section of the steel beam, the type of the column, and the detail of longitudinal reinforcement placement. The specimens were modeled in ABAQUS with solid and truss elements for concrete and steel parts, respectively. In addition, the nonlinear material behavior of the concrete was considered in the model where the concrete damaged plasticity model was assigned. The interaction between concrete and steel was also investigated to capture the structural behavior of the specimens measured from the test. The analysis showed that the concrete section improves the structural performance of the composite beam while preventing the steel beam from bucking. The finite element analysis was not capable of catching the strength degradation at the ultimate state but provided reliable results with overall moment-story drift behavior.

Keywords: Composite beam, Beam-column connection, Permanent steel plate, Finite element analysis; Cyclic loading test.

1. Introduction

Steel-concrete composite members have been widely used in the construction industry because a better performance can be achieved compared to typical reinforced concrete or steel structures. In the construction industry, the composite structures were first investigated and applied in developed countries in the early twentieth century, then this type of structural member has been popular all over the world and gains more attention nowadays `. The reason for increased concern is a statement that the combination of materials can improve structural performance, decrease the cost, and give better resistance to corrosion and fire compared with the traditional reinforced concrete or steel structures [1]. There are different methods of how combinations can be applied to structural members such as composite beams, slabs, columns, frames, and joint regions, thus each method is analyzed separately under different load types [1-14]. Adam et al. [3] conducted an experimental study of strengthened beam-column joints subjected to axial load, and Guo et al. [5] studied steel plate shear wall systems consisting of concrete and steel in composite frames. Also, Hwang et al. [6] and Lee et al. [7] suggested beam-column connections under cyclic loading to investigate the seismic performance of their composite connection systems. Oh et al. [8,9] developed a prestressed steel-concrete composite member with various details for openings and tested it, which showed the effect of prestressing of composites girders. Regarding composites columns, several experimental studies can be considered such as Parra-Montesinos and Wight [10], Wang et al. [11,12]. Especially, Agibayeba et al. [13] tried to use the steel-concrete composite pile system as an energy storage medium in the form of compressed air inside. To enhance the economic feasibility regarding steel material, Ju et al. [14] investigated a hybrid built-up wide flange steel beam that is composed of two different steel materials instead of homogeneous TMCP steel which is typically more expensive than ordinary structural steel.

There are many factors by which the comparison is made between composite structures and traditional reinforced concrete or steel structures. Overall, these aspects can be divided into several groups:

***Corresponding author Deuckhang Lee** *is an associate Professor at Department of Architectural Engineering, Chungbuk National University, South Korea. E-mail: dk@cbnu.ac.kr*

Hyunjin Ju *is an Assistant Professor at School of Architecture and Design Convergence, Hankyong National University, South Korea. E-mail: hju@hknu.ac.kr*

Dong-Uk Choi *is Professor School at School of Architecture and Design Convergence, Hankyong National University, South Korea. E-mail: choidu@hknu.ac.kr*

by structural performance, by considering economic benefits, and by construction process and maintenance. The first category includes the benefits in terms of strength and stiffness because the overall advantage is made up of the strength of each material. In other words, the steel and concrete have high tensile and compressive strength, respectively. As for the construction process, the reinforced concrete structures should be constructed accompanying falsework such as formwork and supporting posts which make the construction cumbersome, while the steel structures are relatively easy to construct. However, advantages of the composite systems include the cost reduction by management minimization and by decreasing overall construction time thanks to the prefabrication of some parts. The cross-section size is also can be reduced through optimized prefabrication thus the composite system is economically preferable. Meanwhile, a composite beam is one of the most common structural members where the wide flange beam is combined with a concrete slab by shear connectors. Beam-column composite joint is also popular in the current construction industry due to the benefits of improvement in strength and stiffness. In addition, there are different designs of the connections that are the subject of the current research.

In the current design practices of steel construction, the size of the wide flange beam is determined based on the negative bending moment and shear force required in the end section of the span. It results in the excessive sectional size of the member in the mid-span because the cross-sectional size of the WFB is larger than required, which leads to inadequate and uneconomical design. Thus, a new composite beam-column system was developed and tested to validate the structural performance of the system. Fig. 1 presents the developed steel-concrete composite beam-column connections utilizing prefabricated permanent steel form. One of the key concepts in the composite connection is the adoption of the permanent steel form as a formwork that provides structural contribution and reduces the effort for the falsework. The design of the beam represents the connection of slab with high strength reinforcing bars with wide flange beam where the concrete with steel form was selectively applied. The permanent steel form should be treated as a fire-proof material to consider the steel form as a structural part contributing to the moment capacity. Thus, it is considered as a steel form to cast concrete section in the negative moment region. The contribution of the steel form to structural performance can be considered as an affirmative secondary effect. In addition, the design utilizes the asymmetric cross-section of the wide flange beam for material saving. For the column design, there are two types applied in this study which are steel reinforced concrete (SRC) and H-steel column. A total of five specimens were validated by the experimental study to identify the structural behavior which can be affected by the key variables such as column type, asymmetry of flange section, and placing type of reinforcement.

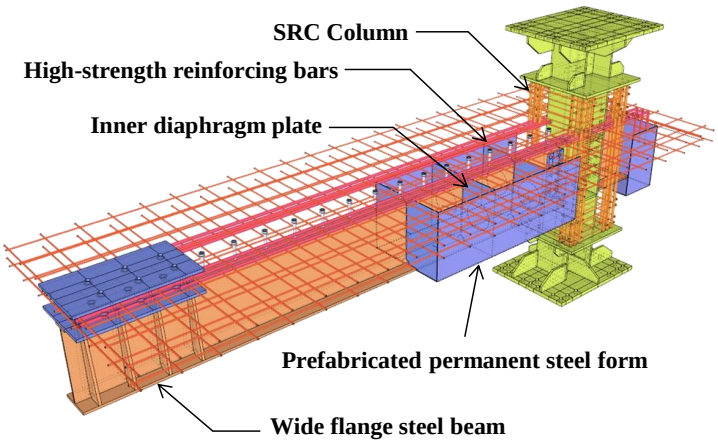

Fig. 1 – Composite beam-column connection with prefabricated permanent steel form

Meanwhile, in most cases where the geometry of the structure is complex, the computer-based numerical approach is preferable in terms of time and budget savings, while laboratory experiments involve a huge amount of resources both material and human, well-equipped facility. In addition, the numerical investigation allows capturing the behavioral mechanism that would be difficult to obtain through the laboratory tests. Despite the advantages of numerical modeling and simulations, the complete study is impossible without the experimental part since the numerical models should be validated by the test results to investigate the simulation results. In other words, the experiment and numerical analyses complement each other [15]. In this study, the performance of the proposed composite system is investigated based on experimental data conducted previously and the finite element method (FEM).

The FEM approach for the composite beam-column connection was suggested by the use of the general analysis program ABAQUS [16].

2. Experimental scheme

2.1 Specimens

The beam-column connection with prefabricated permanent steel form was tested. Prequalified connection details of composite moment-resisting frame specified in the ASCE-7 [17] and AISC [18] were applied referring to a typical beam-column connection of a high-rise office building. The details of the specimens are presented in Fig. 2 and Fig. 3. The total length of specimens is 4500 mm and column height is 2000 mm. The composite beam width is 600 mm in the region of beam-column connection which is supposed to be a negative moment region under gravity load. In addition, the span length is 3500 mm which is the distance between the center of the column to the loading point. All specimens consist of a reinforced concrete slab which is 1600 mm wide and 150 mm thick. Key variables include column and steel beam shapes.

Table 1 presents the details of a total of 5 specimens. Three specimens include steel reinforced concrete (SRC) column with wide flange member inside whereas two specimens have only H shape steel column. The sectional dimension of the SRC column is 600×600 mm with a wide flange member of 300×300×10×15, while the size of H shape steel column is 400×400×13×21 which means the height of 400 mm, flange width of 400 mm, web thickness of 13 mm, and flange thickness of 21 mm. Regarding beams, specimen S1 has a symmetrical wide flange beam of which size is 500×200×200×10×16 which means the height of 500 mm, top flange width of 200 mm, bottom flange width of 200 mm, web thickness of 10 mm, and flange thickness of 16 mm. For all other specimens, the top flange is two times smaller than the bottom flange in width. Another variable is the existence of a diaphragm that is attached to the permanent steel form and steel beam. The diaphragm plate has 200 mm diameter holes to provide composite action between steel and concrete parts in the end region of the span. For specimen S5, longitudinal rebars are designed to be passing by the steel column as an attempt to improve the constructability, whereas in other specimens the longitudinal rebars are welded to the steel column. From the material test, 27 MPa was obtained for compressive strength of concrete. The material properties also include 500 MPa, 325 MPa, and 235 MPa specified yield strength for reinforcement, steel plates, and wide flange beams and steel columns, respectively and the measured steel properties are presented in Table 2.

2.2. Test set-up

A reverse cyclic loading test was performed on a special set-up which represents high stiffness reaction frame connected with the strong floor. The brief experimental scheme is presented in Fig. 4. The column of the specimen was attached on the top and bottom to the high stiffness reaction wall with two pin supports. The load was applied at the end of the beam member in a positive moment direction using a 1000kN capacity actuator. As shown in Fig. 5, the reversed cyclic loading was applied in accordance with ANSI/AISC 341 “Prequalified Connections for Special and Intermediate Steel Moment Frames for Seismic Applications” [19]. Predefined cyclic loading started with the 0.375%, 0.5% and 0.75% drift ratios repeated 6 times. The 1.0% drift ratio was applied 4 times followed by the next drift ratios applied 2 times.

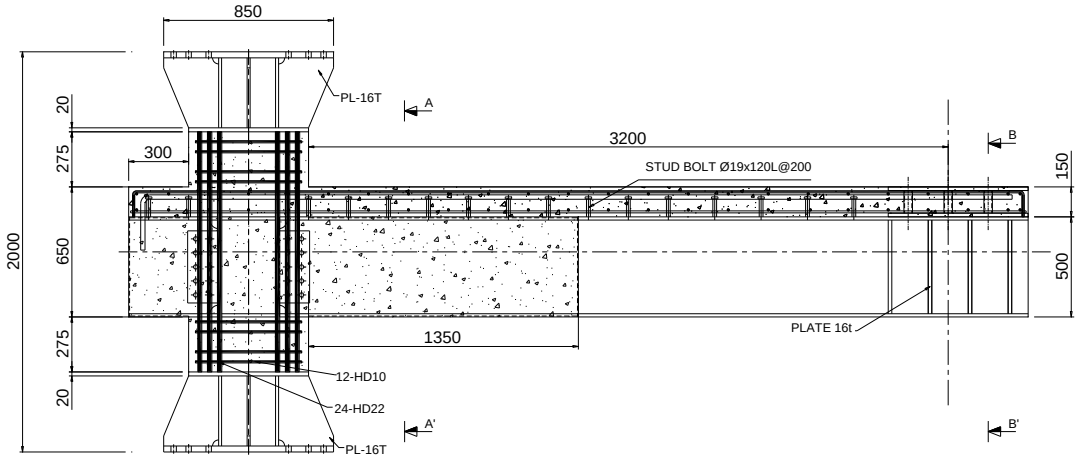

(a) Specimen S1, S2, and S3

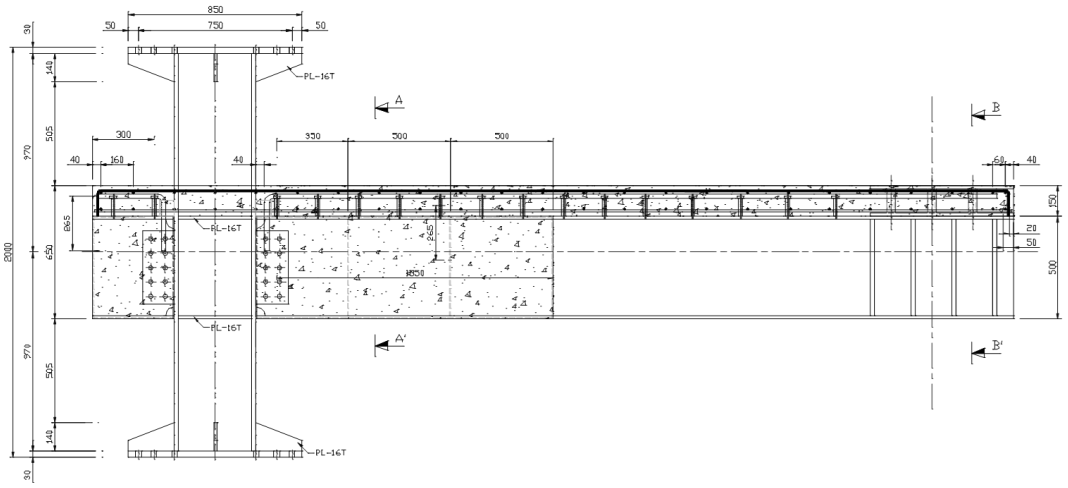

(b) Specimen S4 and S5

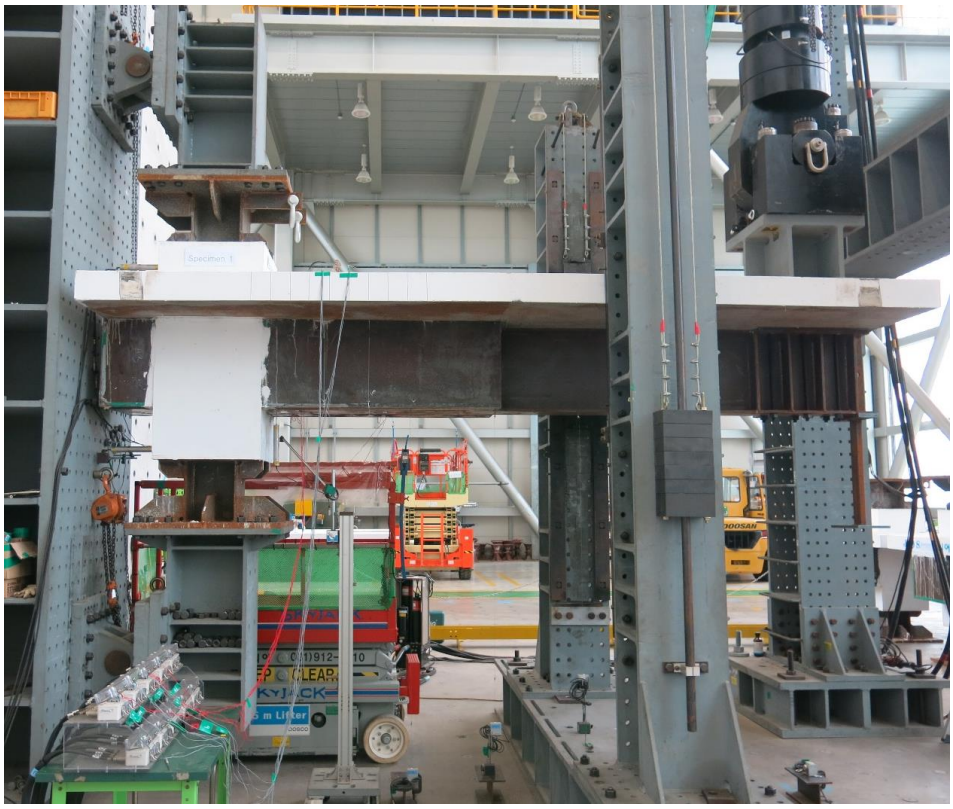

(c) Test set-up S1 specimen

Fig. 2 – Elevation of specimens

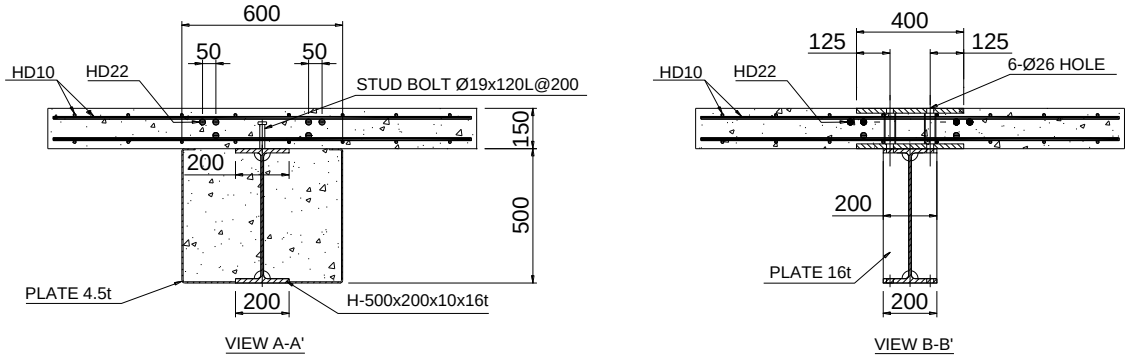

(a) S1 specimen

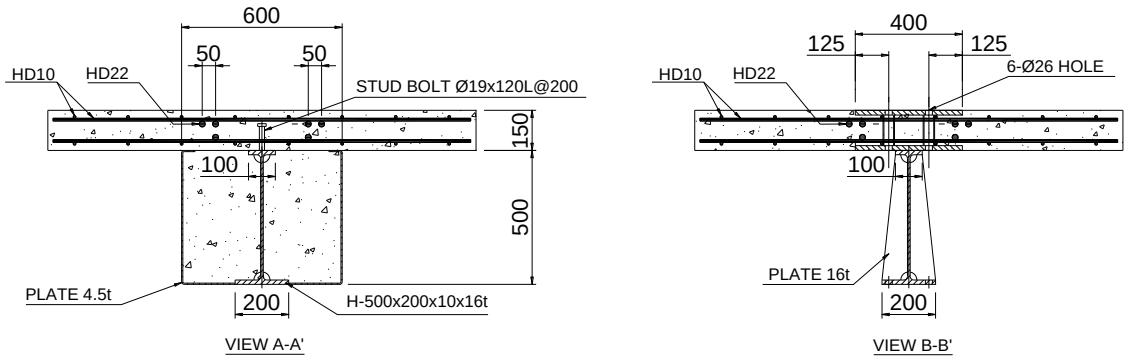

(b) S2 specimen

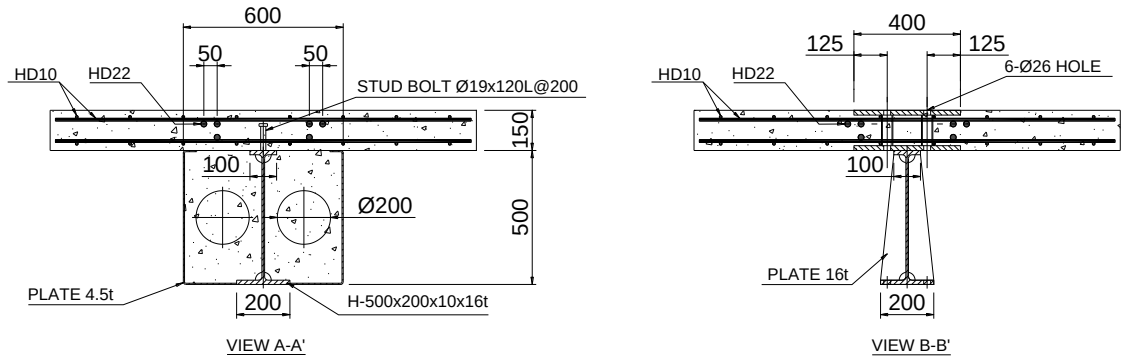

(c) S3 specimen

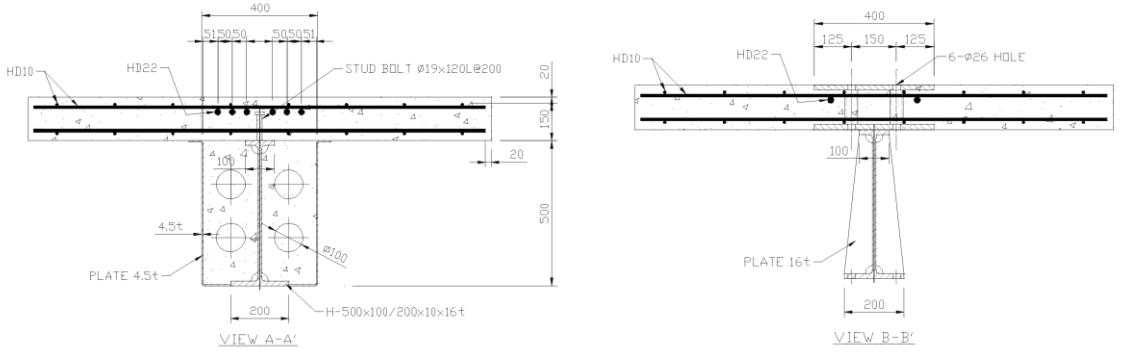

(d) S4 specimen

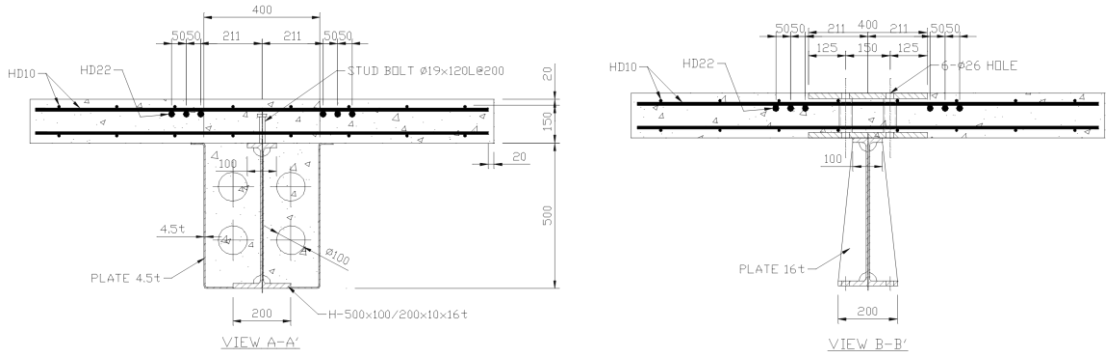

(e) S5 specimen

Fig. 3 – Section details of specimens

To measure the displacement of specimens during the test, LVDTs (linear variable differential transformers) were equipped as shown in Fig. 4 with numbering and strain gages were also attached on reinforcing bars and top and bottom flanges of steel beams. Most of the gages were placed on the beam at 300 mm from the beam column. Two LVDTs (#1 and #2) were located in the connection region to measure shear deformation. Another two LVDTs were attached to the column (#3 and #4) at 200 mm from the beam-column connection to capture rotation angles. LVDTs numbered 6-8 were located along the beam length. One of the LVDTs (#9) was installed at the loading point to record displacement and obtain a story drift ratio.

Table 1 – Design details of test specimens

#	Name	Column type	Concrete strength (MPa)	WFB(SM490)		RC beam size (height×width)	Dia-phragm	Rebar (HD22)
				Column *(H-h×fw×wt×ft)	Beam *(H-h×tfw×bfw×wt×ft)			
1	SRCC+USB	600×600 SRC	24	H-300×300×10×15	H-500×200×200×10×16	600×500	Not in-serted	A
2	SRCC+ASB	600×600 SRC		H-300×300×10×15	H-500×100×200×10×16	600×500	Not in-serted	A
3	SRCC+ASB	600×600 RC		H-300×300×10×15	H-500×100×200×10×16	600×500	Inserted	A
4	SHC+ASB	H-Steel column		H-400×400×13×21	H-500×100×200×10×16	400×500	Inserted	A
5	SHC+ASB	H-Steel column		H-400×400×13×21	H-500×100×200×10×16	400×500	Inserted	P
USB: Uniform Steel Beam ASB: Asymmetric Steel Beam				SRCC: Steel Reinforced Concrete Column; SHC: Steel H-shape Column A: Anchorage; P: Passing by the steel column				

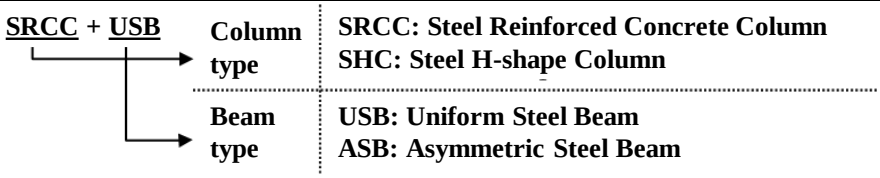

*h: height, tfw: top flange width, bft: bottom flange width, wt: web thickness, ft: flange thickness

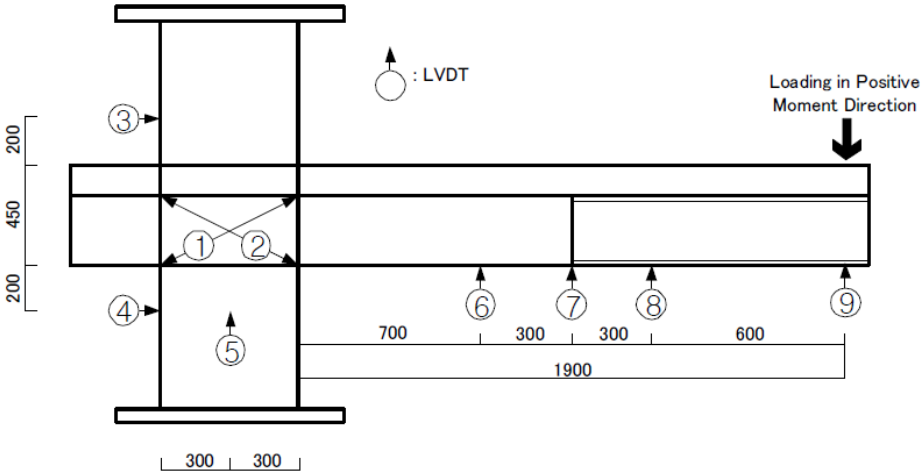

Fig. 4 – LVDTs and gages location

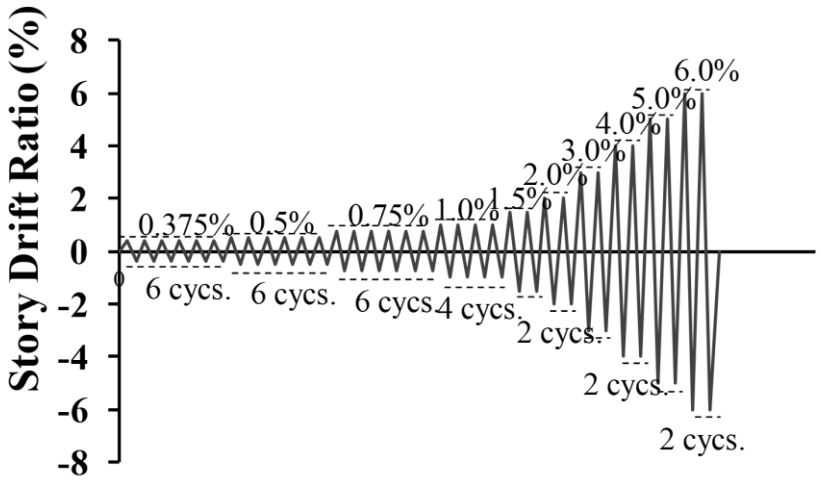

Fig. 5 – Cyclic loading protocol

Table 2 –Steel properties

Type		Yield strength, fy (MPa)	Tensile strength, fu (MPa)
SM 490plate	10 mm	342.9	516.7
	15 mm	339.7	521.4
	16 mm	363.6	624.4
SS400 plate	10 mm	278.2	410.3
Reinforcing bar (Grade 500)	10 mm	548.5	661.9
	22 mm	522.6	731.1

Fig. 6 shows the test results of five specimens and calculated nominal flexural strength for the negative and positive moments. According to AISC design provisions [18], the composite beam-column connection should complete at least one cycle at 4% drift ratio, and the lateral load should not be less than 80% of the nominal strength in both positive and negative directions. The nominal flexural strength was calculated to estimate the strength of specimens. The maximum concrete stain was assumed to be 0.003 and the compressive contribution of concrete was calculated by the equivalent stress block (ACI 318-14 [20]). For steels, the bi-linear stress-strain models were used. The tensile contribution of the concrete was neglected; thus, the top flange of steel beam and high-strength concrete slab reinforcement contributes to the tension forces in the negative direction. On the other hand, the concrete inside permanent steel form and the bottom flange of steel beam provides the compressive forces. With the assumptions, the strength of the composite section under negative and positive bending moments was estimated. Several additional assumptions were also adopted: the effect of the permanent steel form was ignored, and the flexural strength of the composite section subjected to the positive bending moment was estimated considering the section as a T-beam specified in ACI 318. For the strength calculations, the material properties of the test specimens were used. The flexural strength obtained from the test was higher than the nominal strength.

Specimen S1 showed satisfactory seismic performance up to 4% drift ratio with the completion of two cycles. The failure occurred with material separation and SRC column crashing at the first loading cycle of 5% drift ratio. The obtained flexural strength was more than the nominal strength. No stiffness degradation was observed when the first cracks were detected on the top at 0.375% drift ratio. At 0.5% drift ratio, additional cracks were observed in the panel zone which did not affect the overall behavior. The top and bottom flanges at beam-column connection yielded at 0.75% and 1.0% drift ratios, respectively. At 1.5% drift ratio the high-strength reinforcing bars in the concrete slab yielded in the negative direction.

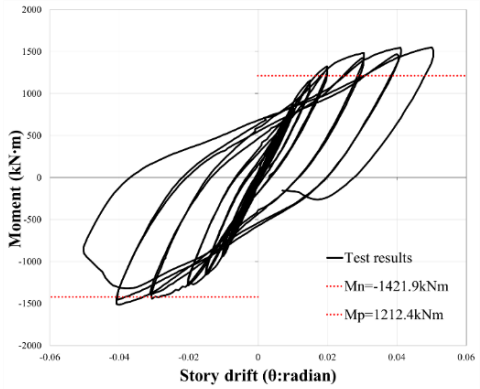

(a) S1 specimen

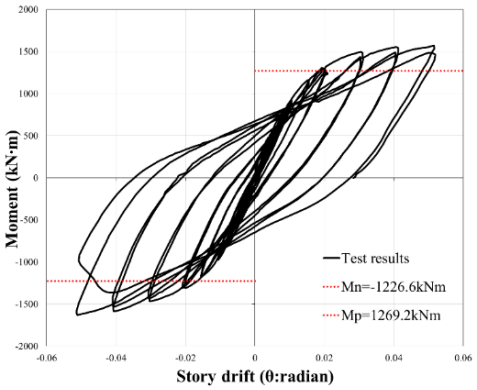

(b) S2 specimen

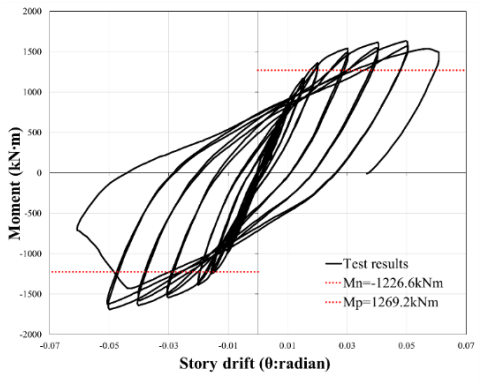

(c) S3 specimen

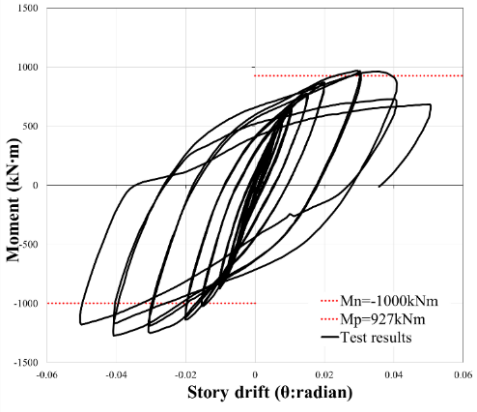

(d) S4 specimen

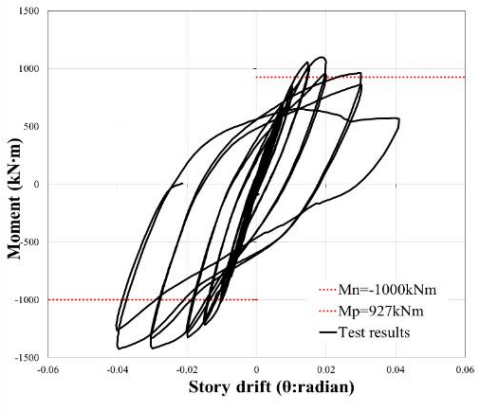

(e) S5 specimen

Fig. 6 – Cyclic responses of test specimens obtained from real test

Details of specimens S2 and S3 are identical to that of specimen S1 except for the asymmetric section of the wide flange beam. In addition, the inner diaphragm was adopted in specimen S3 which means that the simulation modeling and results are the same for S2 and S3. The first cracks were also observed at 0.375% drift ratio like in the S1 specimen followed by the absence of stiffness reduction. Panel zone cracks were observed first at 0.5% drift ratio of positive loading direction. The top and bottom flanges of the beam yielded at 1.0% drift ratio in the negative and positive loading directions, respectively. Beam reinforcement yielded at the same drift ratio. The overall observation of the behavior of specimen S2 shows that the strength and stiffness of the specimen were higher than the calculated nominal strength at 4.0% drift ratio. However, all cycles were fully accomplished until 5.0% drift ratio. Compared to specimen S2, the separation of permanent form and concrete in specimen S3 was not observed before the ultimate state due to inner diaphragm implementation. The final failure of specimen S3 was observed at a higher drift ratio compared to the previous specimens, namely 6.0% drift ratio. For better visualization, the results for S1-S3 specimens are given in Fig. 6. The results are almost the same which means that the implementation of the asymmetric cross-section is assumed to give minimal effect on the performance of the composite structure.

As regards S4 and S5 specimens, the difference in the design is in the H-type column compared to the RC column of previous specimens. The difference between them itself is in the way of the connection of longitudinal reinforcement to the wide flange member of the column. For specimen S4, the strength and stiffness of the specimen were a little bit higher than the calculated nominal strength. All cycles were fully accomplished until 5.0% drift ratio. For specimen S5, all cycles were fully completed at 4.0% drift ratio. Overall, the performance of specimens with an H-type column is lower than the performance of specimens with an RC column.

3. Finite element simulation

3.1 Modeling

The finite element model of the composite beam-column connection was accomplished based on the dimensional details of the specimens. The analysis follows the common nonlinear analysis procedure implemented in ABAQUS/CAE [16]. As shown in Fig. 7(a), a 3D model of the specimen consists of concrete, steel, and reinforcing bars, which are modeled referring to the dimension of specimens., but the model was somewhat simplified. For example, the prefabricated permanent steel form was not modeled because it plays the role of the structurally non-participating formwork. Therefore, specimens S2 and S3 specimens have identical simulation models because the only difference between them is the existence of a diaphragm placed inside of the steel form. In test specimens, stud bolts were placed as shear connectors to connect the concrete slab and steel beam. In the finite element model, instead of modeling the stud bolts, an interaction condition was assigned between two materials, which is one of the key points to accurately simulate the composite beam-column system. The concrete and steel parts were modeled as 3D solid elements (type C3D10) whereas reinforcing bars were molded as truss elements (type T3D2).

Due to the complex shape of the concrete part, the tetrahedral element shape which consists of 10 nodes was implemented for the mesh of the model as shown in Fig. 7(b). The proper mesh size was determined as 90 mm by mesh convergence. The convergence study started with coarser elements with a mesh size of 150 mm followed by a comparison of numerical and experimental results. Then the element size was adjusted until the proper size was found. The tetrahedral element used in modeling has mid-side nodes, thus the analysis is implemented by second-order interpolation. All

other settings related to the element remain as default. The mesh of reinforcing bars is constructed by a 2-node linear element. The mathematical theory based on the Augmented Lagrange constrained enforcement method was assumed to characterize the behavior of each element. Thus, the material assigned to the element remains the same during analysis which properly corresponds to the simulation requirements.

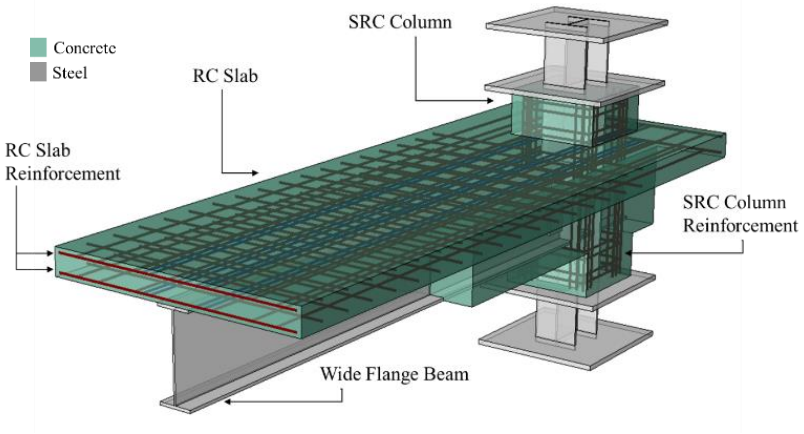

(a) 3D modeling consisting of concrete, steel, and rebars

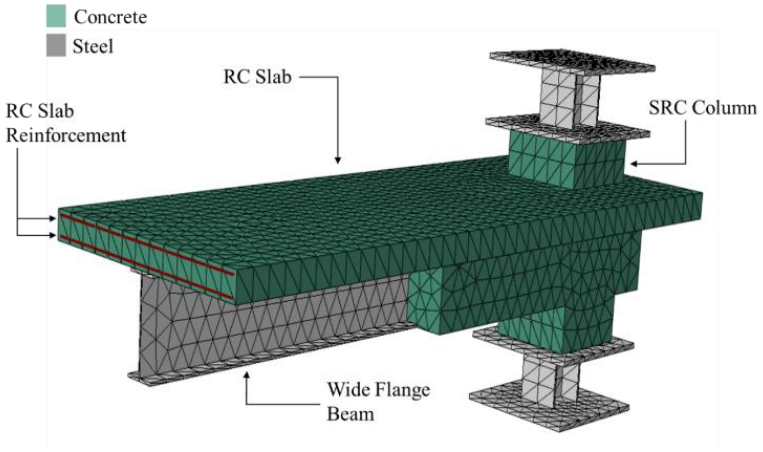

(b) Meshing with tetrahedral elements

Fig. 7 – Finite element modeling

The Augmented Lagrange approach represents the following order of operations in each increment: first, the penalty method is applied by ABAQUS for a converged solution. Then contact pressure is "augmented" in the case when the penetration of the slave node to the master exceeds the tolerance. Iterative calculations are conducted until the converged solution is found. With this approach, the penetration of slave surface can be controlled, and over-constraint can be prevented. The default tolerance factor calculated by the program is five percent of the interface length for surface-to-surface contact. The default penalty stiffness is calculated by increasing the corresponding element stiffness by 1000 times [16].

3.2. Materials assigned

The concrete damaged plasticity (CDP) model was assigned to concrete, which considers nonlinearity and concrete damaged plasticity. It is generally used for concrete structures under cyclic loading. Fig. 8 represents the stress-strain curve for concrete in uniaxial tension and compression which is defined by the CDP model. The stress-strain relationships were assigned referring to the material test results. For the damages, the dilation angle (ψ), eccentricity ratio (ϵ), viscosity (ν), and the axial compressive ratio (f_{b0}/f_{c0}) are assigned as presented in Table 3. The eccentricity represents the rate at which the function approaches asymptote in the hyperbolic surface of plastic potential in the meridional plane. The default value of 0.1 was assigned for the analysis which means that the dilation angle remains the same over the stress variation. The default values of K=2/3 and f_{b0}/f_{c0}=1.16 are also taken [16]. The tensile damage parameter is the ratio of the cracking strain to the total strain, whereas the compressive damage parameter is defined as the ratio between the inelastic

strain and total strain. For steel, a simply bi-linear curve was used to consider hardening behavior accompanied by cyclic loading. The important inputs for concrete and steel are provided in Tables 3 and 4 which are from referecence [16] and material test. It should be noted that the kinematic hardening was considered to simulate the Bauschinger effect in cyclic responses.

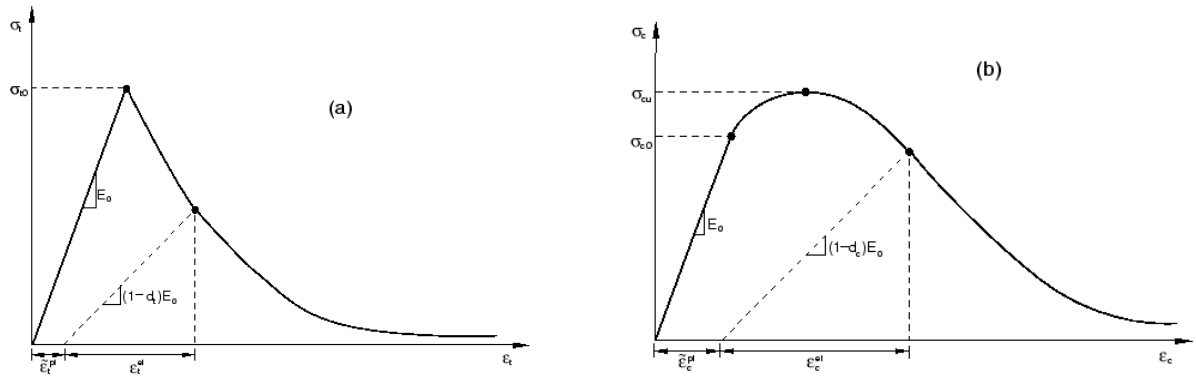

(a) In tension (b) In compression

Fig. 8 – Response of concrete to uniaxial loading

Table 3 –Input data for concrete

Elastic type	Isotropic			
Young's Modulus (MPa)	30000			
Poisson's ratio	0.2			
Concrete damage plasticity				
Dilation angle (degree)	Eccentricity	fb0/fc0	K	Viscosity parameter
38	0.1	1.16	0.67	0.01
Compressive behaviour		Tensile behaviour		
Concrete compression damage		Concrete tension damage		
Tension recovery	0.2	Compression recovery	0.3	

Table 4 –Input data for steel

	Steel		HD10		HD22	
Elastic type	Isotropic		Isotropic		Isotropic	
Young's Modulus (MPa)	200000		200000		200000	
Poisson's ratio	0.3		0.3		0.3	
Plastic hardening	Kinematic		Kinematic		Kinematic	
	Stress (MPa)	Plastic strain	Stress (MPa)	Plastic strain	Stress (MPa)	Plastic strain
	350	0	548.53	0	522.55	0
	517	0.2	661.89	0.16	610.61	0.28

3.3. Interaction

To correctly analyze the structural behavior of composite members, the interaction between two different materials should be appropriately defined, which follows the pure master-slave algorithm in ABAQUS ABAQUS/CAE as shown in Fig. 9. It means that the nodes of the slave surface are not allowed to penetrate the elements of the master surface whereas the opposite is allowed, that is, the master surface can penetrate the slave element. It is important to assign surfaces properly to avoid undesirable overlaps so that ABAQUS can finish a simulation without a convergence issue. It should be noted that the direction of contact is perpendicular to the master surface and that the slave surface can be adjusted after penetration of the master surface. In addition, problems can occur during load application

due to initial shape deformation, thus the contact between master and slave surfaces is also affected. Therefore, for a better contact simulation, it is preferable to assign the high mesh density to the slave surface and the slave adjustment was set to remove the overlap. However, in this study, the type and size of mesh elements for concrete and steel were determined to be the same. In this case, the slave surface should be represented as a softer material in terms of elasticity. Therefore, as shown in Fig. 10, the slave surface and master surface were assigned to the concrete and steel, respectively, because the elasticity of concrete is much lower than steel.

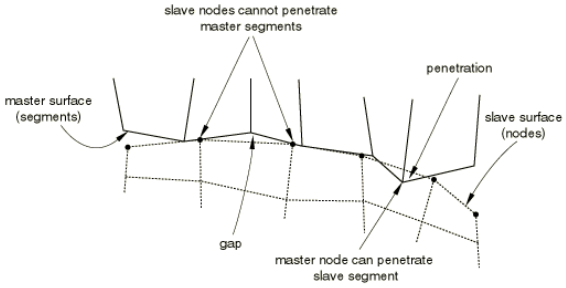

Fig. 9 – Master-slave algorithm [16]

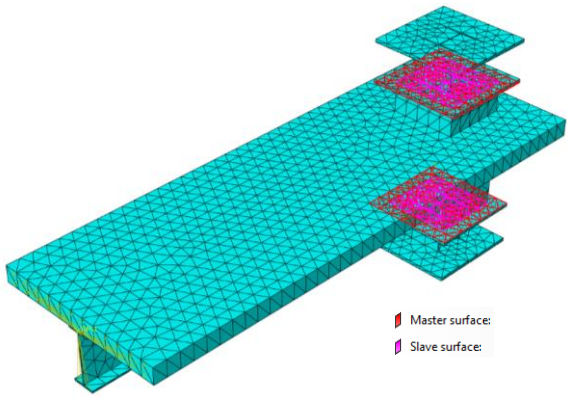

Fig. 10 – Applied Interaction between concrete and steel parts

As for the interaction properties, the tangential and normal behaviors were used with friction formulation of penalty in which friction coefficient was set to be 0.1. Since the connection between the concrete slab and steel wide flange beam was simplified by interaction condition instead of modeling stud bolts, a specific area was assigned to have friction between the top surface of the wide flange beam and concrete slab. The frictionless interaction was also applied to the interface between the concrete column and steel part which is attached to the reaction wall because the overall behavior of the specimen showed a pinching effect that means some slippage between concrete and steel parts. The reinforcing bars were set as an embedded region in the concrete part, thus a fully bonded condition between rebars and surrounding concrete was assumed. In addition, the constrain in the normal direction with frictionless contact was added to prevent any potential separation.

3.4. Load assignment

In the experimental set-up, the reversed cyclic loading was applied by the displacement control of the actuator and the loading point was 3.5 m away from the centerline of the column. In the finite element model, the loading point was assigned to be at the end of the specimen for simplicity as shown in Fig. 11. The coupling constraint was assigned to the surface of the wide flange beam and concrete slab in which the control point is located at the centerline assigning constraints of all degrees of freedom including displacement and rotation. Amplitude input was based on the cyclic loading protocol presented in Fig. 5. To simulate the steel jigs on the top and bottom of the column for specimen fixation, the encastre boundary condition were assigned as shown in Fig. 11 where all the degrees of freedom are constrained (U1 = U2 = U3 = UR1 = UR2 = UR3 = 0).

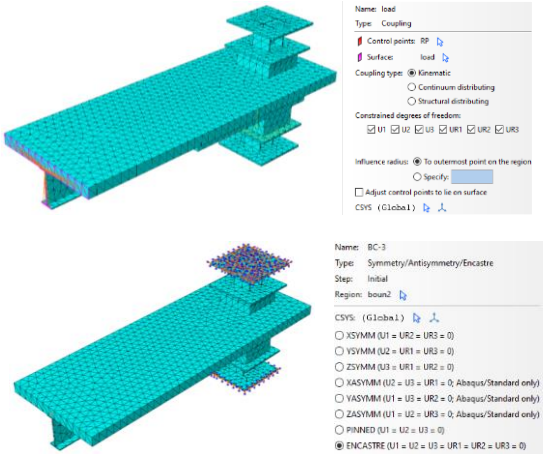

Fig. 11 – Load assignment inputs and boundary condition

4. Simulation result

4.1 Verification of finite element model

To verify the finite element model, a monotonic loading was applied and obtained a backbone curve. Specimen S2 was used as the reference and the comparison of test results and the backbone curve obtained from the monotonic analysis is shown in Fig. 12. The structural behavior is expressed in the relationship of bending moment in negative and positive directions versus story drift. Additionally, the moment-story drift curve for only steel beam-column which consists of wide flange beam and H steel column was also analyzed under cyclic loading and the response is presented in Fig. 12.

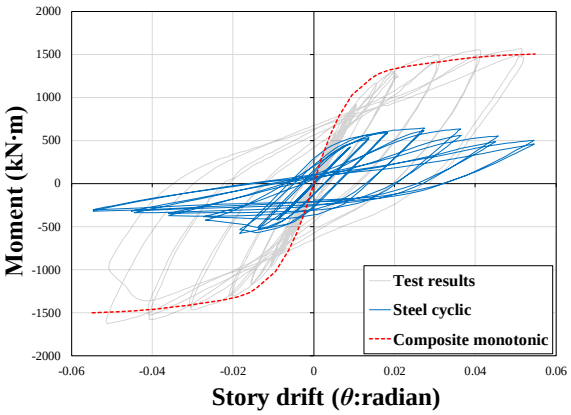

Fig. 12 – Comparison of cyclic responses of test specimens and simulation results for specimen S2

The simulation result of the composite structure under monotonic loading well estimated the overall behavior of the specimen both in negative and positive directions, which suggests that the finite element model was well established and reliable to estimate the structural behavior of the composite beam-column connection in the case of monotonic loading. Regarding the analysis of the steel beam-column case, the simulation result showed a lower strength which is one-third of the strength of the specimen. This is attributed to the not only less sectional area of the steel beam and column compared to the composite member but also the buckling of the steel beam which was observed in the deformation shape of the analysis as shown in Fig. 13. Since there are no experimental data for only steel beam-column, it was estimated by only finite element analysis. On the other hand, the composite beam-column did not have any buckling phenomenon till the maximum capacity was reached, which suggests that the composite structure has improved and stable structural behavior of the beam-column connection by the composite effect. The simulation results estimated the test results of the specimens in a good accuracy in terms of moment-drift ratio behavior, thus the advantages of the composite beam-column connection compared to other structural systems with a single material can be validated from the findings of this study. Also, the detailed experimental study of the suggested composite beam-column connection can be found elsewhere [21].

4.2 Simulation results

Fig. 14 presents the comparison of experimental and simulation data in terms of moment-story drift responses under reversed cyclic loading. The diaphragm inserted in specimen S3 was neglected in the analysis for simplicity and the analysis for specimen S3 is identical to that for specimen S2. Thus, the simulation result for specimen S3 is omitted. From the test results shown in Fig. 5, it turned out that the effect of the diaphragm can be negligible.

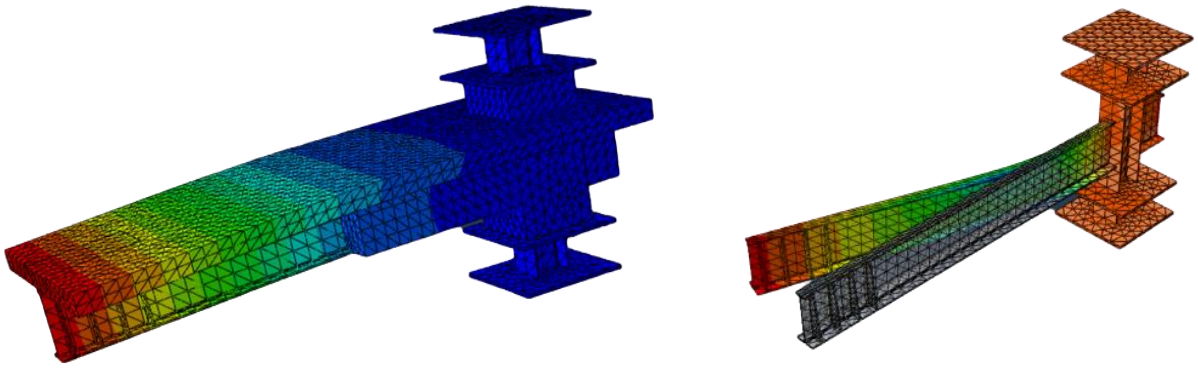

(a) Composite structure (b) Only steel part

Fig. 13 – Specimen S2 model under static loading

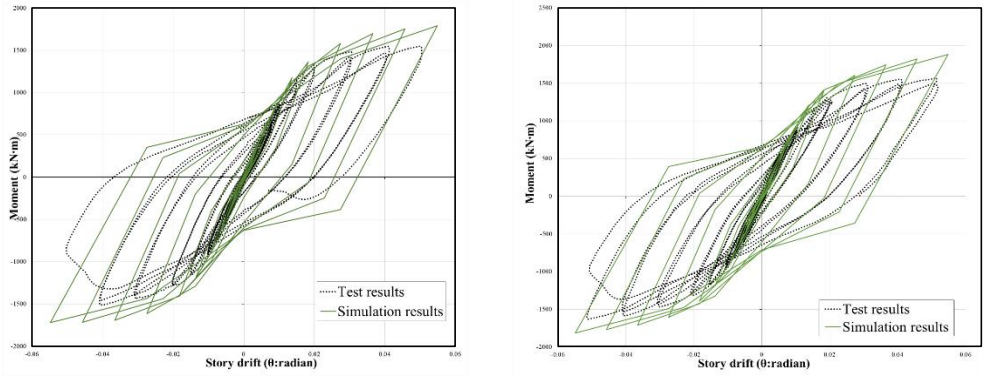

(a) S1 specimen (b) S2 specimen

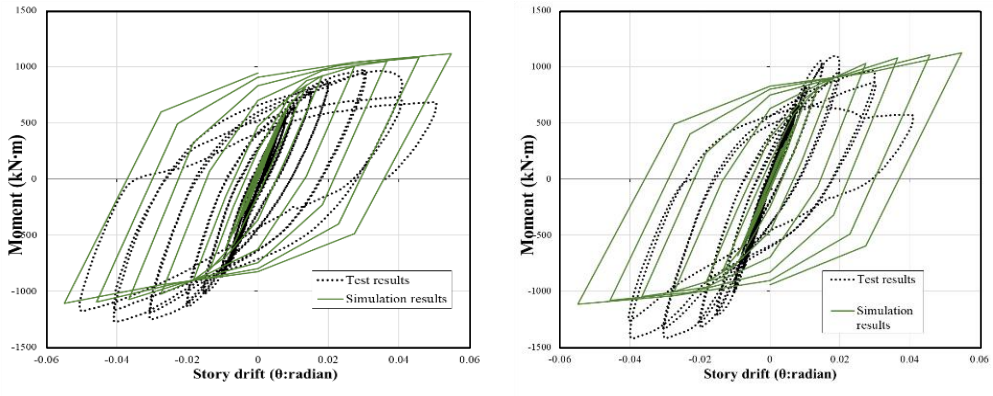

(c) S4 specimen (d) S5 specimen

Fig. 14 – Comparison of test and simulation results for different specimens

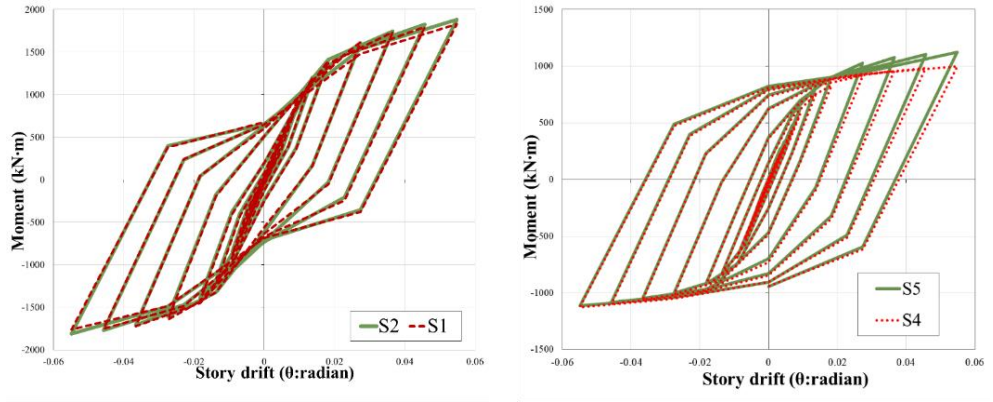

(a) Comparison S1 and S2 (b) Comparison S4 and S5

Fig. 15 – Comparison simulation results of different specimens

.

The simulation showed somewhat exaggerated hysteretic loops, which could be attributed to some assumptions made in the analysis such as material properties. Specifically, the material model for steel is based on the simplification of bilinear hardening rather than elasto-plastic curve, thus in the early stage just after yielding, the stiffness was overestimated and the descending curve of the steel was not considered at the large displacement stage. Also, the assumed contact condition between two materials couldn't be modeled for real considering the bond behavior which would be nonlinear and affected by normal and shear stresses. Thus, the interaction properties and material assignment could be refined in future studies, but the analysis results are acceptable for estimating the test results and investigating the behavioral characteristics of the composite beam-column connection with specimens 1~3. By comparing the finite element simulation results with test results, the discrepancy in strength is less than 15%, which proves the reliability of the finite element model. Comparison between simulation results of specimens is presented in Fig. 15. The simulation results of specimens 1 and 2 are almost the same whereas the sectional area of the wide flange beam in specimen 2 is less than that in specimen 1 by adopting the asymmetric section which has twice less width in top flange compared to the bottom flange. This suggests that the asymmetric wide flange beam is feasible to use for the composite beam-column connection with only minor influence in structural performance. The comparison between specimens 4 and 5 in Fig. 15(b) showed the only difference in strength degradation in the positive moment direction. However, it seems that the analysis did not properly capture the experimental results as shown in Figs. 14(c) and (d). Therefore, further investigation is recommended to capture the effect of reinforcement type when the steel column member is applied.

5. Conclusion

In this study, a finite element analysis was conducted for the steel-concrete composite beam-column connection utilizing prefabricated permanent steel form subjected to cyclic loading. The experiment was previously conducted, and test results were briefly provided and compared to the finite element simulation results. To make the simulation close to the experimental configuration, the analysis phases were carefully implemented including material properties, meshing, and boundary conditions, and loading protocol. From the study, the following conclusions are summarized as follows:

1. The finite element analysis showed quite accurate results compared to experimental data including backbone curve, the flexural strength in positive and negative flexural strength under monotonic and cyclic loadings, which suggests the proposed finite element model can be considered reliable to estimate the structural behavior of the composite beam-column connection.
2. The comparable strengths were obtained for the specimens with symmetric and asymmetric wide flange beams which implies that the high strength reinforcing bars and top flange could reach the strain hardening region based on the larger rotational deformations that occurred in the composite beam member. Thus, the asymmetric section can be utilized considering the structural performance and economic advantages.
3. Specimen 5 showed somewhat higher strength than specimen 4, which could imply the longitudinal reinforcing bar placed to be passing the column has better structural performance while providing better constructability.
4. The strength degradation was more drastic in specimen 5 than specimen 4 and the finite element analysis was not capable of capturing the cyclic responses of specimens 4 and 5, especially it did not catch the strength degradation of specimens. Future research is recommended for better finite element analysis refining the model with the interaction properties and material assignment, which can also include a parametric study to investigate the effect of variation in the connection details.

Acknowledgments

This work was supported by the National Research Foundation of Korea (NRF) grant funded by the Korea government (MSIT) (No. 20203R1F1A1048422 and 2021R1C1C2093437).

References

[1] Johnson, R.P., (2018). Composite Structures of Steel and Concrete: beams, slabs, columns and frames for buildings, John Wiley & Sons, New York, NY, USA, 2018.

[2] Nie, J.G., Wang, J.J., Gou, S.K., Zhu, Y.Y., Fan, J.S., (2019). Technological development and engineering applications of novel steel-concrete composite structures, *Frontiers of Structural and Civil Engineering*, 13, 1, 1-14.

[3] Adarril, J.M., Gimenez, E., Calderon, P.A., Pallares, F.J., Ivorra, S., (2008). Experimental study of beam-column joints in axially loaded RC columns strengthened by steel angles and strips, *Steel and Composite Structures*, 8, 4, 329-342.

[4] Choi, I.R., Park, H.G., (2011). Cyclic Loading Test for Reinforced Concrete Frame with Thin Steel Infill Plate, *Journal of Structural Engineering*, 137, 6, 654-664.

[5] Guo, L.H., Li, R., Rong, Q., Zhang, S.M., (2012). Cyclic behavior of SPSW and CSPSW in composite frame, *Thin-Walled Structures*, 51, 39-52.

[6] Hwang, H.J., Eom, T.S., Park, H.G., Lee, S.H., Kim, H.S., (2015). Cyclic Loading Test for Beam-Column Connections of Concrete-Filled U-Shaped Steel Beams and Concrete-Encased Steel Angle Columns, *Journal of Structural Engineering*, 141, 11,

[7] Lee, D., Kang, T.H.K., Ju, H., Moon, S.W., Yang, I.S., (2019). Seismic Performance of Reinforced Concrete Column-Foundation Connections Using Combo-Type Mechanical Splices, *ACI Structural Journal*, 116, 5, 173-186.

[8] Oh, J.Y., Lee, D.H., Lee, J., Kim, K.S., Kim, S.B., (2016). Experimental Study on Reinforced Concrete Column Incased in Prefabricated Permanent Thin-Walled Steel Form, *Advances in Materials Science and Engineering*, 2016,

[9] Oh, J.Y., Lee, D.H., Cho, S.H., Kang, H., Cho, H.-C., Kim, K.S., (2015). Flexural Behavior of Prestressed Steel-Concrete Composite Members with Discontinuous Webs, *Advances in Materials Science and Engineering*, 2015, 278293.

[10] Parra-Montesinos, G., Wight, J.K., (2000). Seismic response of exterior RC column-to-steel beam connections, *Journal of Structural Engineering*, 126, 10, 1113-1121.

[11] Wang, J.F., Chen, X.Y., Shen, J., (2012). Performance of CFTST column to steel beam joints with blind bolts under cyclic loading, *Thin-Walled Structures*, 60, 69-84.

[12] Wang, Q.W., Shi, Q.X., Tian, H.H., (2016). Experimental study on shear capacity of SRC joints with different arrangement and sizes of cross-shaped steel in column, *Steel and Composite Structures*, 21, 2, 267-287.

[13] Agibayeva, A., Lee, D., Ju, H.J., Zhang, D.C., Kim, J.R., (2021). Application of steel-concrete composite pile foundation system as energy storage medium, *Structural Engineering and Mechanics*, 77, 6, 753-763.

[14] Ju, H., Lee, S.J., Choi, S.M., Kim, J.R., Lee, D., (2020). Applicability of Hybrid Built-Up Wide Flange Steel Beams, *Metals*, 10, 5,

[15] Nethercot, D.A., (2002). The importance of combining experimental and numerical study in advancing structural engineering understanding, *Journal of Constructional Steel Research*, 58, 10, 1283-1296.

[16] Hibbitt, H., Karlsson, B., Sorensen, P., (2011). Abaqus Analysis Users Manual, Version 6.10, Dassault Systemes Simulia, Providence, RI, USA., 2011.

[17] ASCE, (2010). Minimum Design Loads for Buildings and Other Structures, *ASCE/SEI Standard 7-10.*

[18] AISC, (2016). Prequalified Connections for Special and Intermediate Steel Moment Frames for Seismic Applications, *ANSI/AISC 358-16*, Chicago, USA.
[19] AISC, (2005). Seismic provisions for structural steel buildings, *ANSI/ AISC 341-05*, Chicago, USA.
[20] ACI Committee 318, (2014). Building Code Requirements for Structural Concrete and Commentary (ACI 318R-14), *American Concrete Institute*, Farmington Hills, MI, USA.
[21] Yang, I.S., Lee, D., Ju, H., Lee, S.J., Oh, J.Y., (2022). Steel-concrete composite beam-column connections utilizing prefabricated permanent steel form, *Journal of Building Engineering*, 46, 103836.